Dynamical mean-field theory of noisy spiking neuron ensembles: Application to the Hodgkin-Huxley model

Hideo Hasegawa*
Department of Physics, Tokyo Gakugei University, Koganei, Tokyo 184-8501, Japan
(Received 16 April 2003; published 14 October 2003)

A dynamical mean-field approximation (DMA) previously proposed by the present author [H. Hasegawa, Phys. Rev E **67**, 041903 (2003)] has been extended to ensembles described by a general noisy spiking neuron model. Ensembles of N-unit neurons, each of which is expressed by coupled K-dimensional differential equations (DEs), are assumed to be subject to spatially correlated white noises. The original KN-dimensional *stochastic* DEs have been replaced by $K(K+2)$-dimensional *deterministic* DEs expressed in terms of means and the second-order moments of *local* and *global* variables: the fourth-order contributions are taken into account by the Gaussian decoupling approximation. Our DMA has been applied to an ensemble of Hodgkin-Huxley (HH) neurons ($K=4$), for which effects of the noise, the coupling strength, and the ensemble size on the response to a single-spike input have been investigated. Numerical results calculated by the DMA theory are in good agreement with those obtained by direct simulations, although the former computation is about a thousand times faster than the latter for a typical HH neuron ensemble with $N=100$.

DOI: 10.1103/PhysRevE.68.041909 PACS number(s): 87.10.+e, 84.35.+i, 05.45.−a, 07.05.Mh

I. INTRODUCTION

It is well known that a small cluster of cortex may contain thousands of similar neurons. Each neuron, which receives spikes from hundreds of other neurons, generates spikes propagating along the axon towards synapses exciting neurons in the next stage. Dynamics of an individual neuron with voltage-dependent ionic channels can be described by the Hodgkin-Huxley-type (HH) model [1], or by reduced, simplified neuron models such as integrate-and-fire (IF), FitzHugh-Nagumo (FN) [2,3], and Hindmarsh-Rose (HR) models [4]. Although the response of a single neuron *in vitro* is rather accurate, that in *vivo* is not reliable [5]. This is due to noisy environment in living brains, where various kinds of noises are reported to be ubiquitous (for a review see Ref. [6]). In recent years, the population of neuron ensembles has been recognized to play important roles in the information transmission (*pooling effect*) [7–12]. Then it is necessary for us to theoretically investigate high-dimensional, stochastic differential equations (DEs) describing the large-scale noisy neuron ensemble. In order to make our discussion concrete, let us consider ensembles consisting of N-unit neurons, each of which is described by K-dimensional coupled DEs: for example, $K=1$, 2, 3, and 4 for IF, FN, HR, and HH neuron models, respectively. Dynamics of such neuron ensembles, expressed by KN-dimensional *stochastic* DEs, has been so far investigated with the use of the two approaches: (i) direct simulations and (ii) analytical methods, such as the Fokker-Planck equation (FPE) and the moment method. Simulations have been made for large-scale networks mostly consisting of IF neurons. Since the CPU time to simulate networks by conventional methods is proportional to N^2, it is rather difficult to simulate realistic neuron clusters in spite of recent computer development. In the FPE dynamics of neuron ensembles is described by the population activity. Although the FPE is the powerful method formally applicable to the case of arbitrary K and N [13], actual calculations have been made mostly for $N=\infty$ ensembles of a $K=1$ model with the use of the mean-field and/or diffusion approximations [14]. Similar population density approaches have been recently developed for large-scale neuronal clusters [15,16]. The moment method initiated by Rodriguez and Tuckwell (RT) has been applied to single FN [17,18] and HH neurons [19,20]. When the moment method is applied to a single neuron model with K variables, K-dimensional stochastic DEs are replaced by $(1/2)K(K+3)$-dimensional deterministic DEs. When the moment method is applied to N-unit neuron ensembles under consideration, KN-dimensional stochastic DEs are replaced by N_{eq}-dimensional deterministic DEs where $N_{eq}=(1/2)KN(KN+3)$ [17]. For example, in the case of $K=2$ (FN model), the number of equations is $N_{eq}=230$, 20 300, and 2 003 000 for $N=10$, 100, and 1000, respectively. In the case of $K=4$ (HH model), we get $N_{eq}=860$, 80 600, and 8 006 000 for $N=10$, 100, and 1000, respectively. These figures are too large for us to make simulations for realistic neuron clusters. In their subsequent paper of RT [19], they transplanted the result of the moment method for HH neuron ensembles to FPE-type equation which has not been solved yet.

In a previous study (Ref. [21] is hereafter referred to as I), the present author proposed a semianalytical dynamical mean-field approximation (DMA), in which equations of motions for means, variances, and covariances of *local* and *global* variables were derived for N-unit FN neuron ensemble. The original $2N$-dimensional stochastic DEs are replaced by eight-dimensional deterministic DEs: $N_{eq}=8$ is much smaller than corresponding figures in the moment method mentioned above. The DMA calculations in I on the spiking-time precision and the synchronization in FN neuron ensembles are in good agreement with direct simulations. The feasibility of the DMA has been demonstrated in I.

*Email address: hasegawa@u-gakugei.ac.jp

The purpose of the present paper is twofold. The first purpose is to extend the DMA of I to general neuron ensembles subject to white noises described by KN-dimensional stochastic DEs, which will be replaced by $K(K+2)$-dimensional deterministic DEs. The second purpose of the present paper is to apply the generalized DMA to an ensemble of HH neurons, which is more realistic than the FN neuron model previously studied in I. Since Hodgkin and Huxley proposed the HH model in 1952 [1], many studies have been intensively made on properties of the HH model. Responses of a single, pairs, and ensembles HH neurons mostly to direct and sinusoidal currents have been investigated. In recent years, responses of HH neurons to spike-train inputs have been studied [22–25]. The stochastic resonance (SR) of HH neurons for sinusoidal and spike inputs with various kinds of added noises has been investigated [26–33]. These studies have shown that noise can play a constructive role in signal transmission against our conventional wisdom. In most studies on SR, however, noises added to ensemble neurons are considered to be independent of each other. Quite recently effects of spatially correlated noises on SR have been investigated [31], which shows that although common noises work to enhance the synchronization in neuron ensembles, they are not effective for SR, in contrast to independent noises. We will adopt in this study, spatially correlated white noises in order to clarify respective effects of common and independent noises on the response of ensemble neurons.

The paper is organized as follows. In Sec. II, we extend the DMA theory to general neuron ensembles described by KN stochastic DEs. Our DMA theory is applied to HH neuron ensembles in Sec. III. Some numerical results on HH neuron ensembles are presented in Sec. IV. Conclusions and discussions are given in Sec. V.

II. DMA FOR A GENERAL NEURON ENSEMBLE

A. Equation of motions

We assume an ensemble of N-unit neurons ($N \geqslant 2$), each of which is described by K-dimensional nonlinear differential equations (DEs). Dynamics of a given neuron ensemble is expressed by

$$\frac{dv_i}{dt} = F^{(1)}(\{u_{qi}\}) + \left(\frac{w}{N-1}\right) \sum_{j(\neq i)} G(v_j(t)) + K^{(e)}(t) + \xi_i(t), \tag{1}$$

$$\frac{du_{pi}}{dt} = F^{(p)}(\{u_{qi}\}) \quad (p = 2-K), \tag{2}$$

where $v_i = u_{pi}$ with $p=1$ denotes the membrane potential of a neuron i ($=1-N$), u_{pi} with $p=2-K$ stands for auxiliary variables and $F^{(p)}$ is functions of $(\{u_{qi}\})$. The synaptic-coupling strength w is assumed to be constant, $G(v) = 1/\{1 + \exp[-(v-\theta)/\epsilon]\}$ is the sigmoid function with the threshold θ and the width ϵ [34,35], and $K^{(e)}$ stands for an applied external input whose explicit form will be given later [Eq. (56)]. The last term of Eq. (1) expresses the spatially correlated white noises $\xi_i(t)$ given by

$$\langle \xi_i(t) \rangle = 0, \tag{3}$$

$$\langle \xi_i(t)\xi_j(t') \rangle = [\beta_0^2 \delta_{ij} + \beta_1^2 (1-\delta_{ij})]\delta(t-t') = (\beta_C^2 + \beta_I^2 \delta_{ij})\delta(t-t'), \tag{4}$$

where $\beta_C = \beta_1$ and $\beta_I = \sqrt{\beta_0^2 - \beta_1^2}$ denote the magnitudes of common and independent noises, respectively, and the bracket $\langle\ \rangle$ expresses the stochastic average [36]; the case of $\beta_1 = 0$ ($\beta_1 = \beta_0$) stands for independent (common) noises only.

In order to derive DEs in the DMA theory, we first define the global variables for the ensemble by [21]

$$U_p(t) = \frac{1}{N} \sum_i u_{pi}(t), \tag{5}$$

and their averages by

$$\mu_p(t) = \mu_{u_p}(t) = \langle U_p(t) \rangle. \tag{6}$$

Deviations from these averages of local variables are given by

$$\delta u_{pi}(t) = u_{pi}(t) - \mu_{u_p}(t), \tag{7}$$

and those of global variables given by

$$\delta U_p(t) = U_p(t) - \mu_{u_p}(t). \tag{8}$$

Next we define the variances and covariances between local variables given by (argument t is neglected hereafter)

$$\gamma_{p,q} = \gamma_{u_p,u_q} = \frac{1}{N} \sum_i \langle \delta u_{pi} \delta u_{qi} \rangle, \tag{9}$$

and those between global variables given by

$$\rho_{p,q} = \rho_{u_p,u_q} = \langle \delta U_p \delta U_q \rangle. \tag{10}$$

It is noted that γ_{u_p,u_q} expresses fluctuations in local variables, while ρ_{u_p,u_q} those in global variables.

We assume that the noise intensity is weak and that the distribution function $p(\mathbf{z})$ for KN-dimensional random variables of $\mathbf{z} = (\{u_{pi}\})$ is given by the Gaussian distribution concentrated near the mean point of $\boldsymbol{\mu} = (\{\mu_{u_p}\})$ [36]. Numerical simulations have shown that for weak noises, the distribution of $v(t)$ of the membrane potential of a single HH neuron nearly obeys the Gaussian distribution, although for strong noises, the distribution of $v(t)$ deviates from the Gaussian, taking a bimodal form [22,37]. Similar behavior of the membrane-potential distribution has been reported also in a FN neuron model [18,38]. By using Eq. (7), we express Eqs. (1) and (2) in a Taylor expansion of δu_{pi} up to the fourth-order terms. The average yields DEs for the means of $d\mu_{u_p}/dt$ [Eq. (16)]. DEs of variances and covariances may

be obtained by using the equations of motions of δu_{pi}. For example, the DE for $d\gamma_{u_p,u_q}/dt$ is given by

$$\frac{d\gamma_{u_p,u_q}}{dt}=\frac{1}{N}\sum_i\left\langle\left(\frac{\partial\delta u_{pi}}{\partial t}\right)\delta u_{qi}+\delta u_{pi}\left(\frac{\partial\delta u_{qi}}{\partial t}\right)\right\rangle, \quad (11)$$

with

$$\frac{\partial\delta u_{pi}}{\partial t}=\sum_q F^{(u_p)}_{u_q}\delta u_{qi}+\frac{1}{2}\sum_q\sum_r F^{(u_p)}_{u_qu_r}(\delta u_{qi}\delta u_{ri}-\gamma_{u_q,u_r})+\frac{1}{6}\sum_q\sum_r\sum_s F^{(u_p)}_{u_qu_ru_s}\delta u_{qi}\delta u_{ri}\delta u_{ti}+\delta_{p1}\left(\frac{w}{N-1}\right)\times\sum_{k(\neq i)}\left[G_{u_1}\delta u_{1k}+\frac{1}{2}G_{u_1u_1}(\delta u_{1k}^2-\gamma_{1,1})+\frac{1}{6}G_{u_1u_1u_1}\delta u_{1k}^3\right]+\delta_{p1}(K^{(e)}+\xi_i), \quad (12)$$

where q, r, and s run from 1 to K, $F^{(u_p)}=F^{(p)}$, $F^{(u_p)}_{u_q}=\partial F^{(p)}/\partial u_q$, $F^{(u_p)}_{u_qu_r}=\partial^2F^{(p)}/\partial u_q\partial u_r$, and $F^{(u_p)}_{u_qu_ru_s}=\partial^3F^{(p)}/\partial u_q\partial u_r\partial u_s$ are evaluated at the means of $(\{\mu_{u_p}\})$, and similar derivatives for G. In the process of calculations of means, variances, and covariances, we have taken into account the fourth-order moment contributions with the use of the Gaussian decoupling approximation, as given by

$$\langle\delta u_{pi}\delta u_{qi}\delta u_{ri}\delta u_{si}\rangle\simeq\langle\delta u_{pi}\delta u_{qi}\rangle\langle\delta u_{ri}\delta u_{si}\rangle+\langle\delta u_{pi}\delta u_{ri}\rangle\times\langle\delta u_{qi}\delta u_{si}\rangle+\langle\delta u_{pi}\delta u_{si}\rangle\langle\delta u_{qi}\delta u_{ri}\rangle, \quad (13)$$

$$\frac{1}{N}\sum_i\langle\delta u_{pi}\delta u_{qi}\delta u_{ri}\delta u_{si}\rangle\simeq\gamma_{u_p,u_q}\gamma_{u_r,u_s}+\gamma_{u_p,u_r}\gamma_{u_q,u_s}+\gamma_{u_p,u_s}\gamma_{u_q,u_r}, \quad (14)$$

$$\frac{1}{N^2}\sum_i\sum_j\langle\delta u_{pi}\delta u_{qj}\delta u_{rj}\delta u_{sj}\rangle\simeq\rho_{u_p,u_q}\gamma_{u_r,u_s}+\rho_{u_p,u_r}\gamma_{u_q,u_s}+\rho_{u_p,u_s}\gamma_{u_q,u_r}. \quad (15)$$

The importance of including the fourth-order term has been pointed out by Tanabe and Pakdaman [38] in the improved moment method for a noisy FN neuron.

After some manipulations, we get DEs for means, variances, and covariances given by (details being given in Appendix A of I):

$$\frac{d\mu_{u_p}}{dt}=F^{(u_p)}+\frac{1}{2}\sum_q\sum_r F^{(u_p)}_{u_q,u_r}\gamma_{u_q,u_r}+\delta_{p1}[wU_0+K^{(e)}], \quad (16)$$

$$\frac{d\gamma_{u_p,u_q}}{dt}=\sum_r[F^{(u_p)}_{u_r}\gamma_{u_q,u_r}+F^{(u_q)}_r\gamma_{u_p,u_r}]+\beta_0^2\delta_{p1}\delta_{q1}+wU_1[\delta_{p1}\zeta_{u_q,u_1}+\delta_{q1}\zeta_{u_p,u_1}]+\frac{1}{6}\sum_r\sum_s\sum_t[F^{(u_p)}_{u_ru_su_t}(\gamma_{u_q,u_r}\gamma_{u_s,u_t}+\gamma_{u_q,u_s}\gamma_{u_r,u_t}+\gamma_{u_q,u_t}\gamma_{u_r,u_s})+F^{(u_q)}_{u_ru_su_t}(\gamma_{u_p,u_r}\gamma_{u_s,u_t}+\gamma_{u_p,u_s}\gamma_{u_r,u_t}+\gamma_{u_p,u_t}\gamma_{u_r,u_s})], \quad (17)$$

$$\frac{d\rho_{u_p,u_q}}{dt}=\sum_r[F^{(u_p)}_{u_r}\rho_{u_q,u_r}+F^{(u_q)}_{u_r}\rho_{u_p,u_r}]+\left[\frac{1}{N}\beta_0^2+\left(1-\frac{1}{N}\right)\beta_1^2\right]\delta_{p1}\delta_{q1}+wU_1[\delta_{p1}\rho_{u_q,u_1}+\delta_{q1}\rho_{u_p,u_1}]+\frac{1}{6}\sum_r\sum_s\sum_t[F^{(u_p)}_{u_ru_su_t}(\rho_{u_q,u_r}\gamma_{u_s,u_t}+\rho_{u_q,u_s}\gamma_{u_r,u_t}+\rho_{u_q,u_t}\gamma_{u_r,u_s})+F^{(u_q)}_{u_ru_su_t}(\rho_{u_p,u_r}\gamma_{u_s,u_t}+\rho_{u_p,u_s}\gamma_{u_r,u_t}+\rho_{u_p,u_t}\gamma_{u_r,u_s})], \quad (18)$$

with

$$\zeta_{u_p,u_q}=\left(\frac{1}{N-1}\right)(N\rho_{u_p,u_q}-\gamma_{u_p,u_q}), \quad (19)$$

$$U_0=\frac{1}{N}\sum_j\langle G(v_j)\rangle=G+\frac{1}{2}G_{vv}\gamma_{v,v}, \quad (20)$$

$$U_1=G_v+\frac{1}{2}G_{vvv}\gamma_{v,v}, \quad (21)$$

where U_0 expresses output spikes of the ensemble, $v_j=u_{1j}$, and arguments of r, s, and t in the sums run from 1 to K. The original KN-dimensional stochastic DEs are transformed to N_{eq}-dimensional deterministic DEs, where $N_{eq}=K+K(K+1)=K(K+2)$.

B. Property of the DMA

In the preceding section, the DMA has been derived with the use of equations of motions for moments. It is, however, possible to alternatively derive the DMA from the conven-

tional moment method with a reduction in numbers of variables, as was shown in I for FN neuron ensembles. In Appendix A, we present a derivation of the DMA from the moment method for a general neuron ensemble under consideration.

We should note that the noise contribution is β_0^2 in Eq. (17), while it is $[(1/N)\beta_0^2+(1-1/N)\beta_1^2]$ in Eq. (18). When model parameters of β_0, β_1, w, and N are varied, the ratio of $\rho_{v,v}/\gamma_{v,v}$ changes. In particular, in the case of $w=0$, we get

$$\frac{\rho_{v,v}}{\gamma_{v,v}}=\frac{1}{N}+\left(1-\frac{1}{N}\right)\left(\frac{\beta_1}{\beta_0}\right)^2 \tag{22}$$

$$=\frac{1}{N} \quad \text{for} \quad \beta_1=0 \tag{23}$$

$$=1 \quad \text{for} \quad \beta_1=\beta_0. \tag{24}$$

Equation (23) agrees with the *central-limit theorem* for independent noises, while Eq. (24) expresses the result for common noises. On the other hand, in the opposite limit of $w\to\infty$, we get $\rho_{v,v}/\gamma_{v,v}\to 1$. The change in the ratio of $\rho_{v,v}/\gamma_{v,v}$ reflects on the firing-time distributions and the degree of synchronization in neuron ensembles, as will be discussed in the following.

Firing time distributions. The nth firing time of a given neuron i in the ensemble is defined as the time when the membrane potential $v_i(t)$ crosses the threshold θ from below:

$$t_{oin}=\{t|v_i(t)=\theta;\dot{v}_i>0\}. \tag{25}$$

The distribution of firing times of t_{oin} of a given neuron i is given by [17,21]

$$Z_\ell(t)\sim\phi\left(\frac{t-t_o^*}{\delta t_{o\ell}}\right)\frac{d}{dt}\left(\frac{\mu_v}{\sigma_\ell}\right)\Theta(\dot{\mu}_v), \tag{26}$$

with the normal distribution function given by

$$\phi(x)=\frac{1}{\sqrt{2\pi}}\exp\left(-\frac{x^2}{2}\right) \tag{27}$$

and

$$\delta t_{o\ell}=\frac{\sigma_\ell}{\dot{\mu}_v}. \tag{28}$$

Here $\sigma_\ell=\sqrt{\gamma_{v,v}}$ and $\dot{\mu}_v=d\mu_v/dt$ are evaluated at $t=t_o^*$, where $\mu_v(t_o^*)=\theta$. In the limit of vanishing β, Eq. (26) reduces to

$$Z_\ell(t)=\delta(t-t_o^*). \tag{29}$$

Similarly we may define the mth firing time relevant to the global variable $V(t)=(1/N)\Sigma_i v_i(t)$ as [21]

$$t_{gm}=\{t|V(t)=\theta;\dot{V}(t)>0\}. \tag{30}$$

The distribution of firing times of t_{gm} is given by

$$Z_g(t)=\phi\left(\frac{t-t_o^*}{\delta t_{og}}\right)\frac{d}{dt}\left(\frac{\mu_1}{\sigma_g}\right)\Theta(\dot{\mu}_v), \tag{31}$$

with

$$\delta t_{og}=\frac{\sigma_g}{\dot{\mu}_v}, \tag{32}$$

where $\sigma_g=\sqrt{\rho_{v,v}}$. In particular, in the case of no couplings, we get

$$\frac{\delta t_{og}}{\delta t_{o\ell}}=\sqrt{\frac{1}{N}+\left(1-\frac{1}{N}\right)\left(\frac{\beta_1}{\beta_0}\right)^2} \quad \text{for } w=0. \tag{33}$$

Synchronous response. The *synchronization ratio* is defined by [21]

$$S(t)=\frac{(\rho_{v,v}/\gamma_{v,v}-1/N)}{(1-1/N)}=\frac{\zeta_{v,v}}{\gamma_{v,v}}, \tag{34}$$

with

$$\zeta_{v,v}=\left(\frac{1}{N-1}\right)(N\rho_{v,v}-\gamma_{v,v})$$

$$=\frac{1}{N(N-1)}\sum_i\sum_{j(\neq i)}\langle\delta v_i\delta v_j\rangle, \tag{35}$$

expressing the averaged covariance for the variable of $(\{\delta v_i\})$. $S(t)$ changes as the model parameters of β_0, β_1, w, and N are varied. It is easy to see from Eqs. (23) and (24) that $S=0$ (the asynchronous state) for $w=0$ and $\beta_1\ll\beta_0$, while $S=1$ (the completely synchronous state) for $w\gg\beta_0^2$ or $\beta_1=\beta_0$. In particular, for $w=0$, we get

$$S(t)=\left(\frac{\beta_1}{\beta_0}\right)^2 \quad \text{for } w=0, \tag{36}$$

which implies that the synchronization is induced by common noises.

III. DMA FOR HH NEURON ENSEMBLES

Equation of motions

For the HH neuron model ($K=4$), $F^{(p)}$ in Eq. (1) is given by [1,23]

$$F^{(1)}=F^{(v)}(v_i,m_i,h_i,n_i)$$

$$=-\frac{1}{C}[g_{\mathrm{Na}}m_i^3h_i(v_i-v_{\mathrm{Na}})+g_{\mathrm{K}}n_i^4(v_i-v_{\mathrm{K}})$$

$$+g_{\mathrm{L}}(v_i-v_{\mathrm{L}})], \tag{37}$$

$$F^{(p)}=F^{(u_p)}(v_i,u_{pi})$$

$$=-[a_{u_p}(v_i)+b_{u_p}(v_i)]u_{pi}+a_{u_p}(v_i) \quad (p=2\text{–}4). \tag{38}$$

In Eqs. (37) and (38), $u_{1i}=v_i$ expresses the membrane potential of a neuron i, and $u_{2i}=m_i$, $u_{3i}=h_i$, and $u_{4i}=n_i$ denote gate variables of Na and K channels for which $a_{u_p}(v)$ and $b_{u_p}(v)$ $(p=2-4)$ are given by

$$a_m(v)=\frac{0.1(v+40)}{[1-e^{-(v+40)/10}]}, \tag{39}$$

$$b_m(v)=4e^{-(v+65)/18}, \tag{40}$$

$$a_h(v)=0.07e^{-(v+65)/20}, \tag{41}$$

$$b_h(v)=\frac{1}{[1+e^{-(v+35)/10}]}, \tag{42}$$

$$a_n(v)=\frac{0.01(v+55)}{[1-e^{-(v+55)/10}]}, \tag{43}$$

$$b_n(v)=0.125e^{-(v+65)/80}. \tag{44}$$

In Eq. (37), the reversal potentials of Na, K channels and leakage are $v_{\mathrm{Na}}=50$ mV, $v_{\mathrm{K}}=-77$ mV, and $v_{\mathrm{L}}=-54.5$ mV: the maximum values of corresponding conductances are $g_{\mathrm{Na}}=120$ mS/cm^2, $g_{\mathrm{K}}=36$ mS/cm^2, and $g_{\mathrm{L}}=0.3$ mS/cm^2; the capacitance of the membrane is $C=1$ μF/cm^2. From functional forms for $F^{(v)}$ and $F^{(u_p)}$ given by Eqs. (37)–(44), we get $F^{(v)}_{v,v}=0, F^{(u_p)}_{u_q}=F^{(u_p)}_{u_p}\delta_{pq}, F^{(u_p)}_{v,u_q}=F^{(u_p)}_{v,u_p}\delta_{pq}$, and $F^{(u_p)}_{u_p,u_q}=0$. The number of nonvanishing third-order derivatives is six for $F^{(v)}$ [$F^{(v)}_{vmm}$, $F^{(v)}_{vmh}$, $F^{(v)}_{vnn}$, $F^{(v)}_{mmm}$, $F^{(v)}_{nnn}$, and $F^{(v)}_{mmh}$] and two for each $F^{(u_p)}$ $(p=2-4)$ [$F^{(u_p)}_{vvv}$ and $F^{(u_p)}_{vvu_p}$].

After some manipulations with Eqs. (16)–(18), we get DEs for means, variances, and covariances given by $(p,q=2-4)$

$$\frac{d\mu_v}{dt}=F^{(v)}+\frac{1}{2}\sum_{p=2}^{4}\sum_{q=2}^{4}F^{(v)}_{u_pu_q}\gamma_{u_p,u_q}+\sum_{p=2}^{4}F^{(v)}_{vu_p}\gamma_{v,u_p}+wU_0+K^{(e)}, \tag{45}$$

$$\frac{d\mu_{u_p}}{dt}=F^{(u_p)}+\frac{1}{2}F^{(u_p)}_{v,v}\gamma_{v,v}+F^{(u_p)}_{v,u_p}\gamma_{v,u_p}, \tag{46}$$

$$\frac{d\gamma_{v,v}}{dt}=2\left[F^{(v)}_{v}\gamma_{v,v}+\sum_{p=2}^{4}F^{(v)}_{u_p}\gamma_{v,u_p}\right]+\beta_0^2+2wU_1\zeta_{v,v}+X_{v,v}, \tag{47}$$

$$\frac{d\gamma_{v,u_p}}{dt}=(F^{(v)}_{v}+F^{(u_p)}_{u_p})\gamma_{v,u_p}+\sum_{q=2}^{4}F^{(v)}_{u_q}\gamma_{u_q,u_p}+F^{(u_p)}_{v}\gamma_{v,v}+w\zeta_{v,u_p}+X_{v,u_p}, \tag{48}$$

$$\frac{d\gamma_{u_p,u_q}}{dt}=(F^{(u_p)}_{u_p}+F^{(u_q)}_{u_q})\gamma_{u_p,u_q}+F^{(u_p)}_{v}\gamma_{v,u_q}+F^{(u_q)}_{v}\gamma_{v,u_p}+X_{u_p,u_q}, \tag{49}$$

$$\frac{d\rho_{v,v}}{dt}=2\left[F^{(v)}_{v}\rho_{v,v}+\sum_{p=2}^{4}F^{(v)}_{u_p}\rho_{v,u_p}\right]+\left[\frac{1}{N}\beta_0^2+\left(1-\frac{1}{N}\right)\beta_1^2\right]+2wU_1\rho_{v,v}+Y_{v,v}, \tag{50}$$

$$\frac{d\rho_{v,u_p}}{dt}=(F^{(v)}_{v}+F^{(u_p)}_{u_p})\rho_{v,u_p}+\sum_{q=2}^{4}F^{(v)}_{u_q}\rho_{u_q,u_p}+F^{(u_p)}_{v}\rho_{v,v}+wU_1\rho_{v,u_p}+Y_{v,u_p}, \tag{51}$$

$$\frac{d\rho_{u_p,u_q}}{dt}=(F^{(u_p)}_{u_p}+F^{(u_q)}_{u_q})\rho_{u_p,u_q}+F^{(u_p)}_{v}\rho_{v,u_q}+F^{(u_q)}_{v}\rho_{v,u_p}+Y_{u_p,u_q}, \tag{52}$$

with

$$\zeta_{u_p,u_q}=\left(\frac{1}{N-1}\right)(N\rho_{u_p,u_q}-\gamma_{u_p,u_q}), \tag{53}$$

$$U_0=\frac{1}{N}\sum_j\langle G(v_j)\rangle=G+\frac{1}{2}G_{vv}\gamma_{v,v}, \tag{54}$$

$$U_1=G_v+\frac{1}{2}G_{vvv}\gamma_{v,v}, \tag{55}$$

where $F^{(v)}$, $F^{(v)}_v=\partial F^{(v)}/\partial v$, etc., are evaluated at means of $(\mu_v,\mu_m,\mu_h,\mu_n)$. In Eqs. (45)–(52), $X_{v,v}$ and $Y_{v,v}$, etc., denote the contributions from the fourth-order terms, whose explicit expressions are given by Eqs. (B1)–(B6) in Appendix B because they are rather lengthy. Although calculations of the fourth-order terms are rather tedious, they play important roles in stabilizing DEs. This is numerically demonstrated in Appendix B for the case of $N=1$.

The original $4N$-dimensional stochastic DEs given by Eqs. (37) and (38) are transformed to 24-dimensional deterministic DEs given by Eqs. (45)–(52) with Eqs. (B1)–(B6): four means (μ_v, μ_m, μ_h, μ_n), ten moments for local variables ($\gamma_{v,v}$, $\gamma_{m,m}$, $\gamma_{h,h}$, $\gamma_{n,n}$, $\gamma_{v,m}$, $\gamma_{v,h}$, $\gamma_{v,n}$, $\gamma_{m,h}$, $\gamma_{h,n}$, $\gamma_{m,n}$), and ten moments for global variables ($\rho_{v,v}$, $\rho_{m,m}$, $\rho_{h,h}$, $\rho_{n,n}$, $\rho_{v,m}$, $\rho_{v,h}$, $\rho_{v,n}$, $\rho_{m,h}$, $\rho_{h,n}$, $\rho_{m,n}$).

In this section, the DMA for the HH model has been obtained by the method of equations of motions of means, variances, and covariances of local and global variables. We may, however, derive it from the moment method, as mentioned before. In Appendix C, DEs in the moment method are presented for HH model.

We expect that our DMA equations given by Eqs. (45)–(52) and (B1)–(B6) may show much variety depending on model parameters such as the strength of white noise (β_0, β_1) couplings w, and the ensemble size N. In Sec. IV, we will present some numerical DMA calculations, which are

compared with results of direct simulations. The DMA equations have been solved by the fourth-order Runge-Kutta method with a time step of 0.01 ms for the initial conditions of $\mu_v=-65.0$, $\mu_m=0.0528$, $\mu_h=0.597$, $\mu_n=0.317$, and $\gamma_{u_p,u_q}=\rho_{u_p,u_q}=0$ (u_p, $u_q=v$, m, h, and n). Direct simulations have been performed by solving $4N$-dimensional DEs given by Eqs. (37) and (38) by using also the fourth-order Runge-Kutta method with a time step of 0.01 ms. Simulation results are the average of 100 trials otherwise noticed.

IV. CALCULATED RESULTS OF HH NEURON ENSEMBLES

A. Firing-time distribution

In the present study, we pay our attention to the response of the HH neuron ensembles to a single-spike input applied to all neurons in the ensemble, given by

$$K^{(e)}(t)=\left(\frac{I_i}{C}\right)\alpha(t-t_i), \tag{56}$$

with the alpha function

$$\alpha(t)=\left(\frac{t}{\tau_s}\right)e^{(1-t/\tau_s)}\Theta(t), \tag{57}$$

where $\Theta(x)=1$ for $x\geqslant 0$ and 0 otherwise, I_i stands for the magnitude of an input spike, C the membrane capacitance [Eq. (37)], t_i the input time of a spike, and τ_s ($=1$ ms) the time constant of synapses. We get the critical magnitude of $I_{ic}=3.62$ μA/cm^2, below which firings of neuron cannot take place without noises ($\beta_0=\beta_1=0$). We have adopted the value of $I_i=5$ μA/ cm^2 for a study of the response to a suprathreshold input. We express the coupling constant w by $w=J/C$ with J in units of μA/cm^2. The time, voltage, current, and noise intensity are hereafter expressed in units of ms, mV, μA/cm^2, and V/s, respectively, though they are sometimes omitted for simplicity of our explanation. We have adopted parameters of $\theta=0$ mV and $\epsilon=10$ mV in the sigmoid function $G(v)$ such that output U_0 is similar to the result given by the α function [see Fig. 1(a)]. Adopted parameter values of β_0, β_1, J and N will be explained shortly.

Figures 1(a)–1(c) show the time courses of μ_v, $\sigma_\ell(=\sqrt{\gamma_{v,v}})$, and $\sigma_g(=\sqrt{\rho_{v,v}})$, respectively, when a single spike is applied at $t=100$ ms. Solid and dashed curves express the results of the DMA and direct simulations, respectively, which are calculated with parameters of $\beta_0=0.1$, $\beta_1=0$, $J=0$, and $N=100$. States of neurons in an ensemble when an input spike is injected at $t=100$ ms are randomized because noises have been already added since $t=0$. We note that μ_v obtained by the DMA is in very good agreement with that obtained by simulations as shown in Fig. 1(a), where an external input of $K^{(e)}(t)$ and an output of $U_0(t)$ are also plotted. Figures 1(b) and 1(c) show that σ_ℓ and σ_g calculated by the DMA are again in good agreement with those of simulations. We note that the relation given by Eq. (23): $\sigma_g/\sigma_\ell=\sqrt{\rho_{v,v}/\gamma_{v,v}}=1/\sqrt{N}$ valid for $w=J/C=0$, is supported in our numerical calculations.

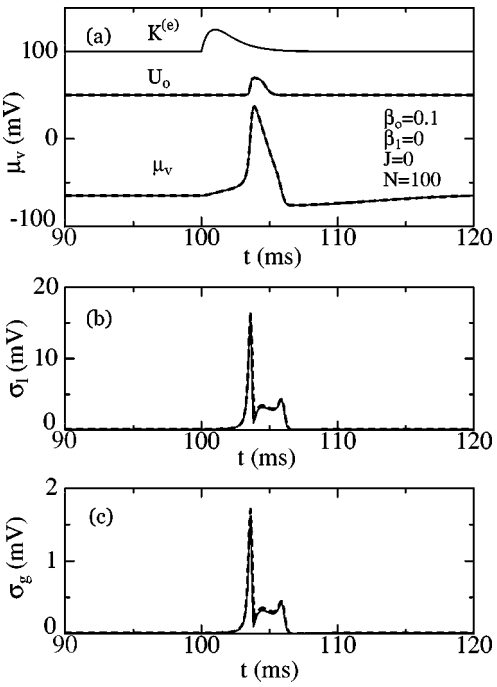

FIG. 1. Time courses of (a) μ_v, (b) σ_ℓ ($=\sqrt{\gamma_{v,v}}$), and (c) σ_g ($=\sqrt{\rho_{v,v}}$) for $\beta_0=0.1$, $\beta_1=0$, $J=0$ and $N=100$, $K^{(e)}$, and U_0 in (a) being shown in arbitrary units.

Figure 2(a) shows Z_ℓ, the firing probability of local variables, which is calculated for $\beta_0=0.1$, $\beta_1=0$, $J=0$, and $N=100$. Firings occur at $t\sim 103.6$ ms with a delay of about 3.6 ms. Fluctuations of firing times of local variable, $\delta t_{o\ell}$, are 0.066 ms in the DMA, while it is 0.069 ms in simulations which is the root-mean-square (RMS) value of firing times defined by Eq. (25). In contrast, Fig. 2(b) shows Z_g, the firing probability of global variables. Fluctuations of firing times of global variable δt_{og} are 0.0066 ms in the DMA and it is 0.0083 ms in simulations, respectively. We note that δt_{og} is much smaller than $\delta t_{o\ell}$ [Eq. (33)].

Noise-strength dependence. When the noise strength is increased, the distribution of membrane potentials is widen and fluctuations of firing times are increased, as was discussed in Sec. II B. Filled squares in Fig. 3(a) show the β_0 dependence of $\delta t_{o\ell}$ obtained by the DMA theory with $\beta_1=0$, $J=0$, and $N=100$, while open squares express the RMS value of firing times obtained by simulations. The agreement between the two methods is fairly good for

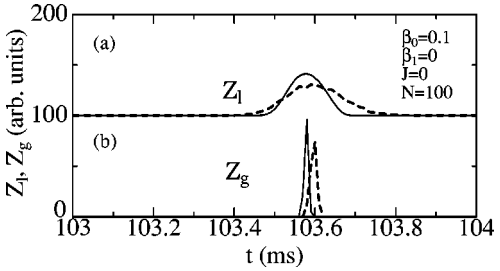

FIG. 2. Time courses of (a) Z_ℓ and (b) Z_g for $\beta_0=0.1$, $\beta_1=0$, $J=0$, and $N=100$. Note the enlarged scale of abscissa compared to that of Fig. 1.

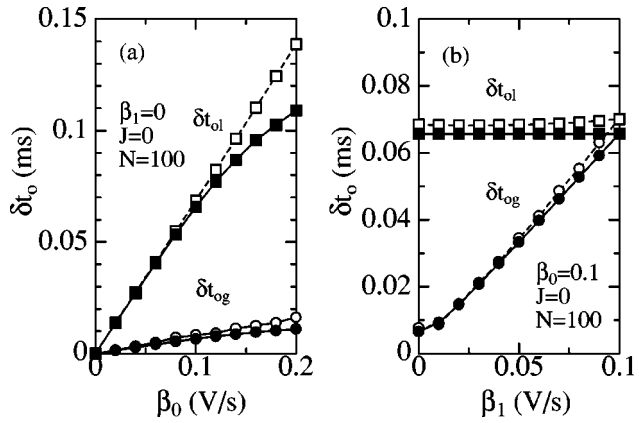

FIG. 3. (a) The β_0 dependence and (b) the β_1 dependence of $\delta t_{o\ell}$ (squares) and δt_{og} (circles) for $\beta_1=0$ in (a) and $\beta_0=0.1$ in (b) with $J=0$ and $N=100$, filled symbols denoting results in the DMA and open symbols those in simulations.

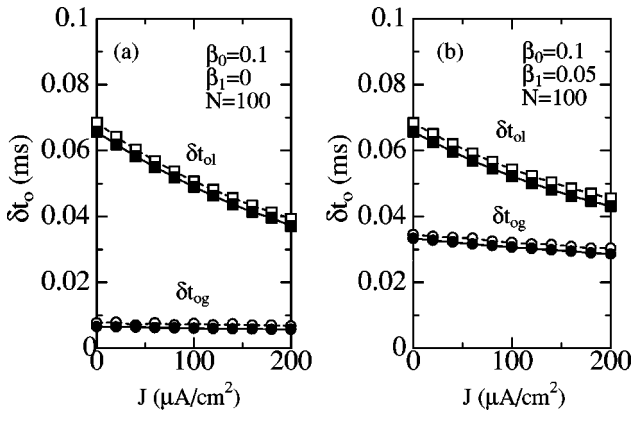

FIG. 5. The J dependence of $\delta t_{o\ell}$ (squares) and δt_{og} (circles) for (a) $\beta_1=0$ and (b) $\beta_1=0.05$ with $\beta_0=0.1$ and $N=100$, filled symbols denoting results in the DMA and open symbols those in simulations.

$\beta_0<0.1$ but becomes worse for $\beta>0.1$. In contrast, filled circles in Fig. 3(a) show the β_0 dependence of δt_{og} relevant to the global variable obtained by the DMA theory and open circles stand for RMS values of firing times in simulations. We note that δt_{og} is much smaller than $\delta t_{o\ell}$ because $\delta t_{og} = \delta t_{o\ell}/\sqrt{N}$ [Eq. (33)].

As β_1 is increased for a fixed β_0, the contribution from common noises increases while that from independent noises decreases ($\beta_C=\beta_1$, $\beta_I=\sqrt{\beta_0^2-\beta_1^2}$). The β_1 dependence of firing-time fluctuations is shown in Fig. 3(b). Filled squares and circles denote the results of $t_{o\ell}$ and t_{og}, respectively, obtained by the DMA, and open squares and circles those by simulations. Figure 3(b) shows that δt_{og} is almost linearly increased as β_1 is increased, while $\delta t_{o\ell}$ remains constant. In the limit of $\beta_1=\beta_0=0.1$, for which only common noises are applied ($\beta_C=0.1$ and $\beta_I=0$), we get $\delta t_{og}=\delta t_{o\ell}$, which shows that common noises do not work to reduce global fluctuations.

Ensemble-size dependence. Filled squares in Fig. 4(a) show the N dependence of $\delta t_{o\ell}$ relevant to local fluctuations

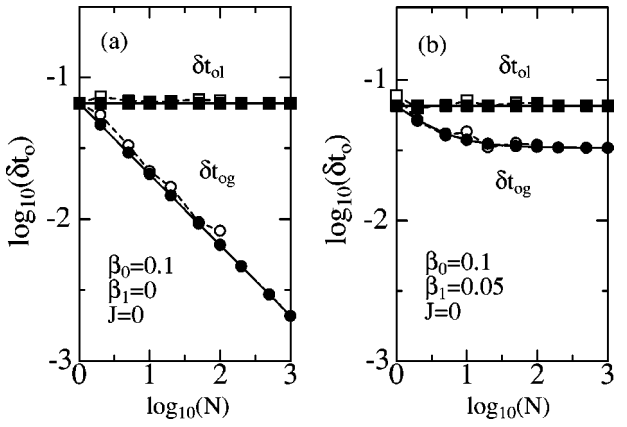

FIG. 4. Log-log plots of $\delta t_{o\ell}$ (squares) and δt_{og} (circles) against N for (a) $\beta_1=0$ and (b) $\beta_1=0.05$ with $\beta_0=0.1$ and $J=0$, filled symbols denoting results in the DMA and open symbols those in simulations.

for $\beta_0=0.1$, $\beta_1=0$, and $J=0$, obtained by the DMA theory, while open squares express that obtained by simulations. We note that $\delta t_{o\ell}$ is independent of N because of no couplings ($J=0$). In contrast, δt_{og} relevant to global fluctuations inversely decreases when the size N is increased, as shown by filled and open circles which are obtained by the DMA theory and simulations, respectively. The relation $\delta t_{og} \propto (1/\sqrt{N})$ holds as given by Eq. (33) for $\beta_1=0$. Figure 4(b) shows a similar plot for a finite value of $\beta_1=0.05$ with $\beta_0=0.1$ and $J=0$. In the limit of $N\to\infty$, the ratio of $\delta t_{og}/\delta t_{o\ell}$ approaches a finite value of $\beta_1/\beta_0=0.5$ [Eq. (33)].

Coupling-strength dependence. So far we have neglected the coupling of J, which is now introduced. Filled squares in Fig. 5(a) show the J dependence of $\delta t_{o\ell}$ calculated by the DMA theory for $\beta_0=0.1$, $\beta_1=0$, and $N=100$, while open squares that obtained by simulations. Filled and open circles express δt_{og} in the DMA theory and simulations, respectively. We note that $\delta t_{o\ell}$ is much reduced as J is increased although there is little change in δt_{og}. Figure 5(b) shows a similar plot of the J dependence of firing time accuracy for finite $\beta_1=0.05$ with $\beta_0=0.1$ and $N=100$. Again a reduction in $\delta t_{o\ell}$ with increasing J is more significant than that in δ_{og}.

B. Synchronization ratio

One of the important effects of the couplings is to yield synchronous firings in ensemble neurons. Figures 6(a) and 6(b) show the time course of the synchronization ratio $S(t)$ for $J=100$ and 200 μA/cm^2, respectively, with $\beta_0=0.1$, $\beta_1=0$, and $N=100$: solid and dashed curves denote the results of the DMA and simulations, respectively. Fairly large fluctuations in simulation results are due to a lack of trial number of 100, which is the limit of our computer facility. A comparison between Figs. 6(a) and 6(b) shows that $S(t)$ is increased as J is increased: the maximum value of $S(t)$ in Fig. 6(b) is $S_{max}=0.019$ which is larger than $S_{max}=0.007$ in Fig. 6(b). Figure 6(c) shows the time course of $S(t)$ for a finite $\beta_1=0.05$ with $\beta_0=0.1$, $J=100$, and $N=100$. A significant increase in S is realized at $100\lesssim t\lesssim 120$ ms which is induced by an applied spike [note the difference in vertical

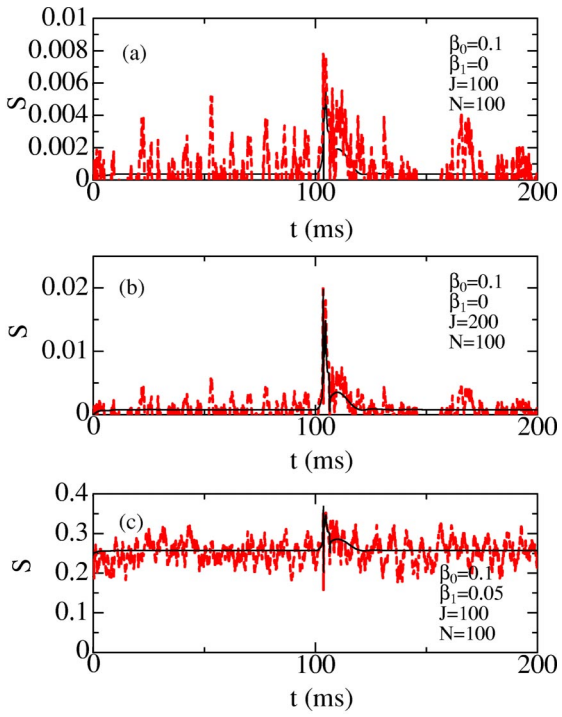

FIG. 6. The time course of synchronization ratio S for (a) $\beta_0=0.1$, $\beta_1=0$, and $J=100$, (b) $\beta_0=0.1$, $\beta_1=0$, and $J=200$, and (c) $\beta_0=0.1$, $\beta_1=0.05$, and $J=100$ with $N=100$, the solid curve denoting results of the DMA and the dashed curve those of simulations.

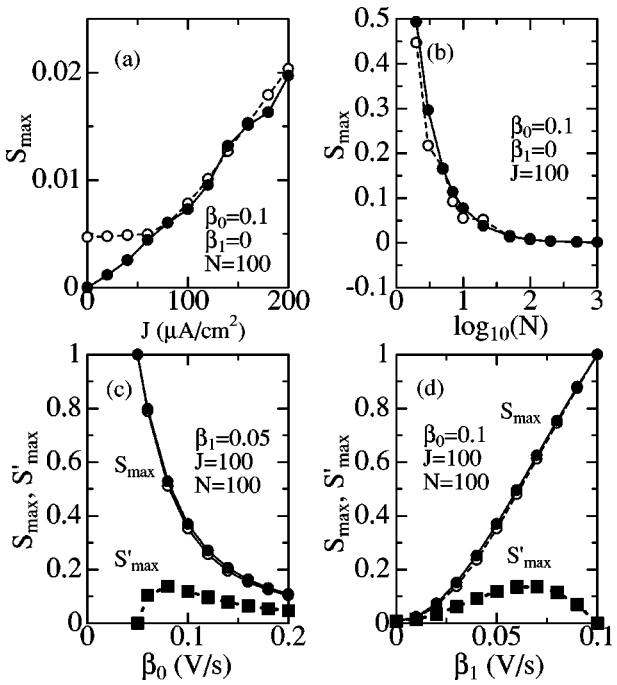

FIG. 7. The dependence of the maximum of the synchronization ratio on (a) J, (b) N, (c) β_0, and (d) β_1; filled and open circles denote S_{max} of the DMA and simulations, respectively, and filled squares express S'_{max} of the DMA (see text).

scales of Figs. 6(a)–6(c)]. We note a fairly large value of $S=0.25$ even without an applied input spike at $t\lesssim 100$ or $t\gtrsim 120$. This expresses the synchronization among the membrane potentials of ensemble neurons induced by added noises although they do not induce firings. In order to distinguish the synchronization with firings from that without firings, we define the firing-induced synchronization ratio, $S'(t)$, given by

$$S'(t)=S(t)-S_b, \tag{58}$$

where $S_b=(\beta_1/\beta_0)^2$ denotes the *background* synchronization induced by noises only [Eq. (36)]. We get $S_{max}=0.369$, $S'_{max}=0.119$, and $S_b=0.25$ in Fig. 6(c). From a comparison of Fig. 6(c) with Fig. 6(a), we note that $S'(t)$ is also much increased by common noises.

An increase in $S(t)$ by an increase of J is clearly shown in Fig. 7(a), where the maximum of $S(t)$ (S_{max}) is plotted as a function of J. A disagreement between results of the DMA and simulations for $J<50$ is due to fluctuations in simulations because of insufficient trial number as mentioned above. The dependence of S_{max} on the size N is shown in Fig. 7(b), where $\beta_0=0.1$, $\beta_1=0$, and $J=100$. S_{max} is decreased with increasing N. Figure 7(c) expresses the β_0 dependence of S_{max} for $\beta_1=0.05$, $J=100$ and $N=100$. At $\beta_0=\beta_1=0.05$, we get $S_{max}=1$, which is decreased as increasing β_0. Filled squares in Fig. 7(c) denote S'_{max}, which shows the maximum around $\beta_0\sim 0.08$. In contrast, Fig. 7(d) show the β_1 dependence of S_{max} for $\beta_0=0.1$, $J=100$ and $N=100$. S_{max} is increased with increasing β_1, and approaches unity as $\beta_1\rightarrow\beta_0(=0.1)$. We note that S'_{max} has the maximum at $\beta_1\sim 0.07$.

V. CONCLUSIONS AND DISCUSSION

In the preceding section, we have reported DMA calculations for a single spike input to HH neuron ensembles. DMA calculations and simulations have shown that (a) $\delta t_{o\ell}$ increases with increasing β_0, or decreasing J, independently of β_1 and N; (b) δt_{og} increases with increasing β_0 or β_1, and decreasing N or J; and (c) S_{max} increases with increasing β_1 or J, or decreasing β_0 or N.

In order to understand these behaviors, we have tried to obtain phenomenological, analytical expressions for $\delta t_{o\ell}$, δt_{og}, and S_{max} as functions of β_0, β_1, J, and N. For small J, we express $\gamma_{v,v}$ and $\rho_{v,v}$ in a power series of J at $t=t_o^*$ where neurons fire, given by (see Appendix E of I [34])

$$\gamma_{v,v}\propto\beta_0^2(1-a_1J+\cdots), \tag{59}$$

$$\rho_{v,v}\propto\beta_0^2\left[\frac{1}{N}+\left(1-\frac{1}{N}\right)\left(\frac{\beta_1}{\beta_0}\right)^2-\left(\frac{b_1}{N}\right)J+\cdots\right]. \tag{60}$$

It is noted that in the limit of $J=0$ ($w=0$), Eqs. (59) and (60) reduce to Eq. (22). Substituting Eqs. (59) and (60) into Eqs. (28) and (32), we get

$$\delta t_{o\ell}\propto\beta_0\left(1-\frac{1}{2}a_1J\right), \tag{61}$$

$$\delta t_{og} \propto \beta_0 \left[\left(\frac{1}{N} + \left(1 - \frac{1}{N} \right) \left(\frac{\beta_1}{\beta_0} \right)^2 \right)^{1/2} - \left(\frac{b_1}{2\sqrt{N}} \right) J \right]. \quad (62)$$

Equations (61) and (62) may explain the behavior of $\delta t_{o\ell}$ and δt_{og} in points (a) and (b) mentioned above.

Next we will obtain the analytical expression for S_{max}. For small J, we get $\gamma_{v,v}$ and $\rho_{v,v}$ in a power series of J at $t = t_o^{(m)}$, where $S(t)$ takes the maximum value, given by (see Appendix E of I [34])

$$\gamma_{v,v} \propto \beta_0^2 (1 - a_2 J + \cdots), \quad (63)$$

$$\rho_{v,v} \propto \beta_0^2 \left[\frac{1}{N} + \left(1 - \frac{1}{N} \right) \left(\frac{\beta_1}{\beta_0} \right)^2 - \left(\frac{b_2}{N} \right) J + \cdots \right]. \quad (64)$$

Substituting Eqs. (63) and (64) into Eq. (34), we get

$$S_{\max} = \left(\frac{\beta_1}{\beta_0} \right)^2 + \left[b_1 \left(\frac{\beta_1}{\beta_0} \right)^2 + \left(\frac{a_2 - b_2}{N - 1} \right) \right] J + \cdots. \quad (65)$$

Equation (65) is consistent with the point (c): S_{max} increases with increasing β_1 and J, or decreasing β_0 and N. Equation (65) shows that in the case of $\beta_1 = 0$, S_{max} is independent of β_0, which is supported in the DMA calculation and simulations (not shown). Expressions given by Eqs. (61), (62), and (65) are useful in a phenomenological sense. In principle, expressions as given by Eqs. (59) and (60) may be derived from DMA equations given by Eqs. (45)–(52), although we have not unfortunately succeeded in getting them because of their complexity.

Numerical calculations in Sec. IV have been made for the response to a single-spike input. The DMA is, however, applicable to arbitrary inputs. This will be demonstrated by adding spike trains to HH neuron ensembles, given by

$$K^{(e)}(t) = \left(\frac{I_i}{C} \right) \sum_n \alpha(t - t_{in}), \quad (66)$$

where t_{in} expresses the nth input time. Figures 8(a) and 8(b) show the time courses of μ_v and σ_ℓ $(= \sqrt{\gamma_{v,v}})$, respectively, for Poisson spike trains with the average interspike interval (ISI) of 25 ms; solid and dashed curves express results of the DMA and simulations, respectively, for $\beta_0 = 0.1$, $\beta_1 = 0$, $J = 0$, and $N = 100$. The time course of μ_v of the DMA is in good agreement with that of simulations. A comparison between the input $K^{(e)}$ and output U_0 shows that when the ISI of input is shorter than about 10 ms, HH neurons cannot respond because of the refractory period [23]. Figures 8(b) shows that σ_ℓ of the DMA is also in good agreement with that of simulations.

To summarize, the DMA theory previously proposed for FN neuron ensemble in I has been generalized to an ensemble described by KN-dimensional stochastic DEs, which has been replaced by $K(K+2)$-dimensional deterministic DEs expressed by means and second-order moments: contributions from the fourth-order moments are taken in account by the Gaussian decoupling approximation. The DMA has been applied to HH neuron ensembles, for which we get

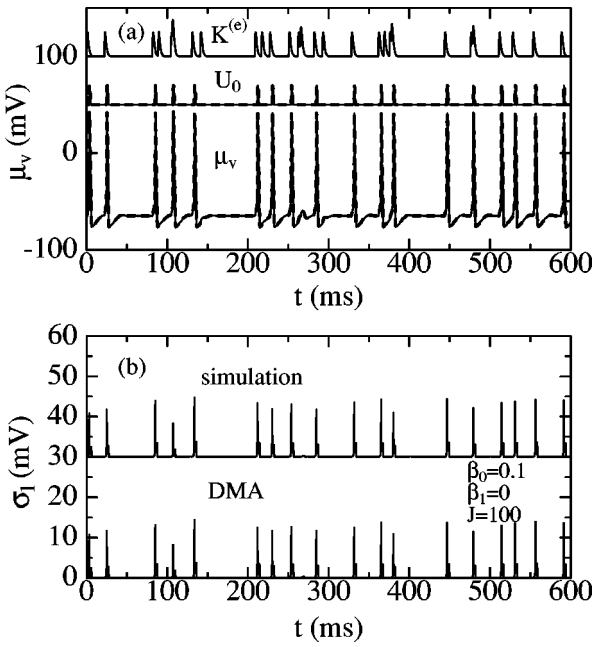

FIG. 8. Time courses of (a) μ_v and (b) $\gamma_{v,v}$ for Poisson spike inputs with the average ISI of 25 ms for $\beta_0 = 0.1$, $\beta_1 = 0$, $J = 0$, and $N = 100$, solid and dashed curves in (a) denoting results of the DMA and simulations, respectively. $K^{(e)}$ and U_o in (a) are plotted in arbitrary units. The result of simulations in (b) is shifted upwards by 30.

24-dimensional deterministic DEs. We have studied effects of noise, the coupling strength, and the ensemble size on the firing-time precision and the firing synchronization for single-spike inputs, obtaining the following results: (i) the firing-time accuracy of the order of one-tenth ms is possible in a large-scale HH neuron ensemble, even without couplings; (ii) the spike transmission is improved with the synchronous response by increasing the coupling strength; and (iii) the synchronization is increased by common noises but decreased by independent noises.

Results (i) and (ii) are consistent with the SR results in HH neuron ensembles [28–33]. Although they are quite similar to the case of FN model discussed in I, their *quantitative* discussions are possible with the use of the realistic HH model. Result (iii) agrees with the result of Ref. [31] for SR in HH neuron ensembles subject of common and independent noises.

Our calculations have demonstrated the feasibility of the DMA, whose advantages may be summarized as follows: (1) because of the semianalytical nature of the DMA, some results may be derived without numerical calculations; (2) the DMA is free from the weak-coupling constraint although it assumes weak noises; (3) a tractable small number of DEs makes calculations feasible for large-scale neuron ensembles with a fairly short computational time; (4) the DMA may be applicable to ensembles with fluctuations not only due to noises but also due to some inhomogeneities in model parameters; and (5) the DMA can be applied to more general stochastic systems besides neuron models.

As for point (3), we may indicate that, for example, the CPU time of DMA calculations for a 200 ms time course of

a $N=100$ HH neuron ensemble with the use of 1.8-GHz PC is 2 s, which is about 2500 times faster than the CPU time of 85 min ($\sim$5000 s) for direct simulations with 100 trials. It is necessary to stress the importance of the fourth-order contributions in stabilizing solutions of the DMA, which is numerically demonstrated in Appendix B. Although expressions for the fourth-order contributions are lengthy, we are much benefited from them once they are derived and planted into computer programs [39]. We are now under consideration to incorporate the time delay in the coupling terms in Eq. (1), with which the HH neuron ensemble may show the intriguing behavior like chaos. Such calculations will be reported in a separate paper.

ACKNOWLEDGMENTS

The author would like to express his sincere thanks to Professor Hideo Nitta for critical reading of the manuscript. This work was partly supported by a Grant-in-Aid for Scientific Research from the Japanese Ministry of Education, Culture, Sports, Science and Technology.

APPENDIX A: DERIVATION OF THE DMA FROM THE MOMENT METHOD FOR GENERAL NEURON ENSEMBLES

In the moment method, we define the means, variances, and covariances given by [17]

$$m_{u_p}^i=\langle u_{pi}\rangle, \tag{A1}$$

$$C_{u_p,u_q}^{i,j}=\langle \Delta u_{pi}\Delta u_{qj}\rangle, \tag{A2}$$

where $\Delta u_{pi}=u_{pi}-m_{u_p}^i$. Assuming the weak couplings and adopting the Gaussian decoupling approximations for the fourth-order moments, we get DEs for general neuron ensembles described by Eqs. (1) and (2):

$$\frac{dm_{u_p}^i}{dt}=F^{(u_p)}+\frac{1}{2}\sum_q\sum_r F_{u_{qi},u_{ri}}^{(u_p)}C_{u_q,u_r}^{(i,i)}+\delta_{p1}\left[\left(\frac{w}{N-1}\right)\sum_{k(\neq i)}\left(G+\frac{1}{2}G_{u_{1k}u_{1k}}C_{u_1,u_1}^{k,k}\right)+K^{(e)}\right], \tag{A3}$$

$$\begin{aligned}\frac{dC_{u_p,u_q}^{i,j}}{dt}=&\sum_r\left[F_{u_{ri}}^{(u_p)}C_{u_q,u_r}^{i,j}+F_{u_{rj}}^{(u_q)}C_{u_p,u_r}^{i,j}\right]+\left[\beta_0^2\delta_{ij}+\beta_1^2\times(1-\delta_{ij})\right]\delta_{p1}\delta_{q1}+\delta_{p1}\left(\frac{w}{N-1}\right)\sum_{k(\neq i)}G_{u_{1k}}C_{u_q,u_1}^{j,k}\\&+\delta_{q1}\left(\frac{w}{N-1}\right)\sum_{k(\neq j)}G_{u_{1k}}C_{u_p,u_1}^{i,k}+\frac{1}{6}\sum_r\sum_s\sum_t\left[F_{u_{ri}u_{si}u_{ti}}^{(u_p)}\left(C_{u_r,u_s}^{i,i}C_{u_t,u_q}^{i,j}+C_{u_r,u_t}^{i,i}C_{u_s,u_q}^{i,j}+C_{u_s,u_t}^{i,i}C_{u_r,u_q}^{i,j}\right)\right.\\&+F_{u_{rj}u_{sj}u_{tj}}^{(u_q)}\left(C_{u_r,u_s}^{j,j}C_{u_t,u_p}^{j,i}+C_{u_r,u_t}^{j,j}C_{u_s,u_p}^{j,i}+C_{u_s,u_t}^{j,j}C_{u_r,u_p}^{j,i}\right)\Big],\end{aligned} \tag{A4}$$

where $F^{(u_p)}=F^{(p)}$, $F_{u_{ri}}^{(u_p)}=\partial F^{(p)}/\partial u_{ri}$, and $F_{u_{ri}u_{si}u_{ti}}^{(p)}=\partial^{(3)}F^{(p)}/\partial u_{ri}\partial u_{si}\partial u_{ti}$ are evaluated for the means of $(\{m_{u_p}^i\})$, and the last term in Eq. (A4) denotes the fourth-order contribution. The number of DEs is $N_{eq}=KN+(1/2)KN(KN+1)=(1/2)KN(KN+3)$.

In order to derive the DMA from the moment method, we define the quantities given by

$$\overline{\mu}_\kappa=\frac{1}{N}\sum_i m_\kappa^i, \tag{A5}$$

$$\overline{\gamma}_{\kappa,\lambda}=\frac{1}{N}\sum_i C_{\kappa,\lambda}^{i,i}+d_{\kappa,\lambda}, \tag{A6}$$

$$\overline{\rho}_{\kappa,\lambda}=\frac{1}{N^2}\sum_i\sum_j C_{\kappa,\lambda}^{i,j}\quad(\kappa,\lambda=u_p,u_q), \tag{A7}$$

where

$$d_{\kappa,\lambda}=\frac{1}{N}\sum_i \delta m_\kappa^i\delta m_\lambda^i, \tag{A8}$$

$$\delta m_\kappa^i=m_\kappa^i-\mu_\kappa. \tag{A9}$$

We may show that Eqs. (A3) and (A4) with Eqs. (A5)–(A7) yield Eqs. (16)–(18): $\overline{\mu}_\kappa=\mu_\kappa$, $\overline{\gamma}_{\kappa,\lambda}=\gamma_{\kappa,\lambda}$, and $\overline{\rho}_{\kappa,\lambda}=\rho_{\kappa,\lambda}$. Then the moment method yields the same results as the DMA as far as the averaged quantities are concerned (see also Appendix B of I).

APPENDIX B: THE FOURTH-ORDER CONTRIBUTIONS IN THE DMA FOR HH NEURON ENSEMBLES

The fourth-order contributions given by $X_{\kappa,\lambda}$ and $Y_{\kappa,\lambda}$ $(\kappa,\lambda=v,u_p)$ in Eqs. (45)–(52) are expressed by

$$\begin{aligned}X_{v,v}=&F_{vmm}^{(v)}(\gamma_{v,v}\gamma_{m,m}+2\gamma_{v,m}\gamma_{v,m})+F_{vmh}^{(v)}(\gamma_{v,v}\gamma_{m,h}+2\gamma_{v,m}\gamma_{v,h})+F_{vnn}^{(v)}(\gamma_{v,v}\gamma_{n,n}+2\gamma_{v,n}\gamma_{v,n})\\&+F_{mmm}^{(v)}\gamma_{v,m}\gamma_{m,m}+F_{nnn}^{(v)}\gamma_{v,n}\gamma_{n,n}+F_{mmh}^{(v)}(\gamma_{v,h}\gamma_{m,m}+2\gamma_{v,m}\gamma_{m,h}),\end{aligned} \tag{B1}$$

$$\begin{aligned}X_{v,u_p}=&\frac{1}{2}[F_{vmm}^{(v)}(\gamma_{v,u_p}\gamma_{m,m}+2\gamma_{u_p,m}\gamma_{v,m})+F_{vmh}^{(v)}(\gamma_{v,u_p}\gamma_{m,h}+\gamma_{u_p,m}\gamma_{v,h}+\gamma_{u_p,h}\gamma_{v,m})+F_{vnn}^{(v)}(\gamma_{v,u_p}\gamma_{n,n}\\&+2\gamma_{u_p,n}\gamma_{v,n})+F_{mmm}^{(v)}\gamma_{u_p,m}\gamma_{m,m}+F_{nnn}^{(v)}\gamma_{u_p,n}\gamma_{n,n}\end{aligned}$$

$$+F^{(v)}_{mmh}(\gamma_{u_p,h}\gamma_{m,m}+2\gamma_{u_p,m}\gamma_{m,h})+F^{(u_p)}_{vvv}\gamma_{v,v}\gamma_{v,v}$$
$$+F^{(u_p)}_{vvu_p}(\gamma_{v,u_p}\gamma_{v,v}+2\rho_{v,v}\gamma_{v,u_p})], \quad \text{(B2)}$$

$$X_{u_p,u_q}=\frac{1}{2}[F^{(u_p)}_{vvv}\gamma_{v,u_q}\gamma_{v,v}+F^{(u_q)}_{vvv}\gamma_{v,u_p}\gamma_{v,v}+(F^{(u_p)}_{vvu_p}+F^{(u_q)}_{vvu_q})$$
$$\times(\gamma_{u_p,u_q}\gamma_{v,v}+2\gamma_{v,u_q}\gamma_{v,u_p})], \quad \text{(B3)}$$

$$Y_{v,v}=F^{(v)}_{vmm}(\rho_{v,v}\gamma_{m,m}+2\rho_{v,m}\gamma_{v,m})+F^{(v)}_{vmh}(\rho_{v,v}\gamma_{m,h}$$
$$+\rho_{v,m}\gamma_{v,h}+\rho_{v,h}\gamma_{v,m})+F^{(v)}_{vnn}(\rho_{v,v}\gamma_{n,n}+2\rho_{v,n}\gamma_{v,n})$$
$$+F^{(v)}_{mmm}\rho_{v,m}\gamma_{m,m}+F^{(v)}_{nnn}\rho_{v,n}\gamma_{n,n}+F^{(v)}_{mmh}(\rho_{v,h}\gamma_{m,m}$$
$$+2\rho_{v,m}\gamma_{m,h}), \quad \text{(B4)}$$

$$Y_{v,u_p}=\frac{1}{2}[F^{(v)}_{vmm}(\rho_{v,u_p}\gamma_{m,m}+2\rho_{u_p,m}\gamma_{v,m})+F^{(v)}_{vmh}(\rho_{v,u_p}\gamma_{m,h}$$
$$+\rho_{u_p,m}\gamma_{v,h}+\rho_{u_p,h}\gamma_{v,m})+F^{(v)}_{vnn}(\rho_{v,u_p}\gamma_{n,n}$$
$$+2\rho_{u_p,n}\gamma_{v,n})+F^{(v)}_{mmm}\rho_{u_p,m}\gamma_{m,m}+F^{(v)}_{nnn}\rho_{u_p,n}\gamma_{n,n}$$
$$+F^{(v)}_{mmh}(\rho_{u_p,h}\gamma_{m,m}+2\rho_{u_p,m}\gamma_{m,h})+F^{(u_p)}_{vvv}\rho_{v,v}\gamma_{v,v}$$
$$+F^{(u_p)}_{vvu_p}(\gamma_{v,u_p}\gamma_{v,v}+2\rho_{v,v}\gamma_{v,u_p})], \quad \text{(B5)}$$

$$Y_{u_p,u_q}=\frac{1}{2}[F^{(u_p)}_{vvv}\rho_{v,u_q}\gamma_{v,v}+F^{(u_p)}_{vvu_p}(\rho_{u_p,u_q}\gamma_{v,v}+2\rho_{v,u_q}\gamma_{v,u_p})$$
$$+F^{(u_q)}_{vvv}\rho_{v,u_p}\gamma_{v,v}+F^{(u_q)}_{vvu_q}(\rho_{u_p,u_q}\gamma_{v,v}$$
$$+2\rho_{v,u_p}\gamma_{v,u_q})], \quad \text{(B6)}$$

where $F^{(v)}_{vmh}=\partial^3F^{(v)}/\partial v\,\partial m\,\partial h$, etc. Although calculations and computer programming of fourth-order contributions given by Eqs. (B1)–(B6) are rather tedious, they play important roles in stabilizing the solution of DEs [39].

Here we demonstrate the importance of the fourth-order contributions in the case of a single HH neuron ($N=1$) for which $w=0$, $\gamma_{\kappa,\lambda}=\rho_{\kappa,\lambda}$, and $X_{\kappa,\lambda}=Y_{\kappa,\lambda}$ in Eqs. (45)–(52) and (B1)–(B6). Figure 9(a) shows the time course of μ_v for $\beta_0=0.1$ and $\beta_1=0$ when the constant input of $I_i=10\ \mu$A/cm^2 is applied at $t=0$ ms. The solid and dashed curves express the results of the DMA and the simulation (100 trials), respectively. The dotted curve denotes the result of the DMA2 (the second-order DMA) in which the fourth-order contributions are neglected ($X_{\kappa,\lambda}=Y_{\kappa,\lambda}=0$). For $t<60$ ms, all results seem to be in good agreement. At $t\gtrsim 60$, however, the solution of the DMA2 becomes unstable and significantly deviates from those of DMA and the simulation. From the time course of $\sigma_\ell=\sqrt{\gamma_{v,v}}$ shown in Fig. 9(b), we note that such deviation of the DMA2 already starts from $t\sim 30$ ms. The solution of the DMA2 is stable at $\beta\leqslant 0.037$ for the constant current of $I_i=10\ \mu$A/cm^2.

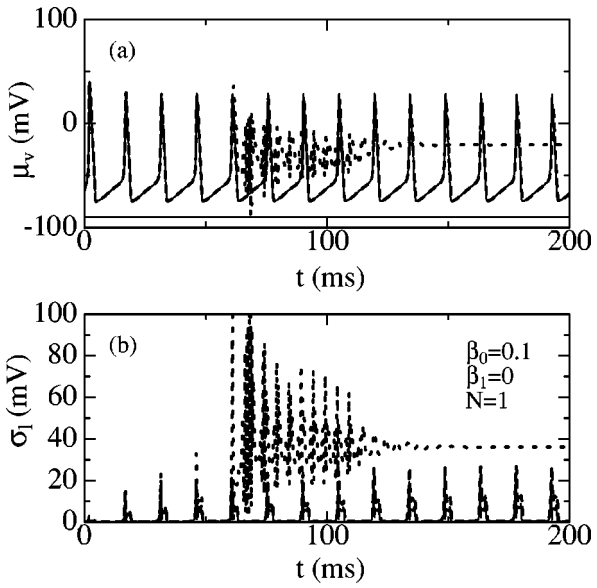

FIG. 9. Time courses of (a) μ_v and (b) $\sigma_\ell(=\sqrt{\gamma_{v,v}})$ with $\beta_0=0.1$, $\beta_1=0$, and $N=1$ for constant current input of $I_i=20$, solid, dotted, and dashed curves denoting results of the DMA, DMA2 (the second-order DMA), and simulations, respectively. A constant input current is shown at the bottom of (a) (see text).

Figures 10(a) and 10(b) show the time courses of μ_v and σ_ℓ for $\beta_0=0.2$ and $\beta_1=0$ when we apply the periodic spike train input given by Eq. (66) with $I_i=5\ \mu$A/cm^2 and a constant ISI of 25 ms. Figure 10(b) clearly shows that the result of the DMA2 deviates from those of the DMA and simulations from the first spike-input, and that the result of the DMA2 diverges at the second spike input. The solution of the DMA2 is stable only at $\beta\leqslant 0.178$ for this periodic spike.

APPENDIX C: THE MOMENT METHOD FOR HH NEURON ENSEMBLES

We will derive DEs in the moment method for HH neuron ensembles, defining the means, variances, and covariances given by [17]

$$m^i_v=\langle v_i\rangle, \quad \text{(C1)}$$

$$m^i_{u_p}=\langle u_{pi}\rangle, \quad \text{(C2)}$$

$$C^{i,j}_{v,v}=\langle\Delta v_i\Delta v_j\rangle, \quad \text{(C3)}$$

$$C^{i,j}_{v,u_p}=\langle\Delta v_i\Delta u_{pi}\rangle, \quad \text{(C4)}$$

$$C^{i,j}_{u_p,u_q}=\langle\Delta u_{pi}\Delta u_{qj}\rangle, \quad \text{(C5)}$$

where $\Delta v_i=v_i-m^i_v$ and $\Delta u_{pi}=u_{pi}-m^i_{u_p}$. Adopting the

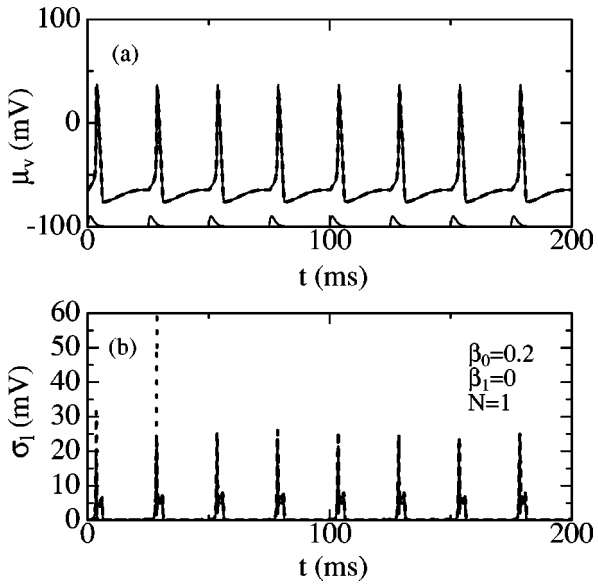

FIG. 10. Time courses of (a) μ_v and (b) $\sigma_\ell(=\sqrt{\gamma_{v,v}})$ with $\beta_0=0.2$, $\beta_1=0$ and $N=1$ for a periodic spike train input with an ISI of 25 ms; solid, dotted, and dashed curves denoting results of the DMA, the DMA2 (the second-order DMA), and simulations, respectively. A periodic input spike is shown at the bottom of (a) (see text).

weak-coupling approximation and the Gaussian approximation for the fourth-order terms, we get DEs given by

$$\frac{dm_v^i}{dt}=F^{(v_i)}+\frac{1}{2}\sum_{p=2}^{4}\sum_{q=2}^{4}F^{(v_i)}_{u_p,u_q}C^{i,i}_{u_p,u_q}+\sum_{p=2}^{4}F^{(v_i)}_{v,u}C^{i,i}_{v,u_p}+\left(\frac{w}{N-1}\right)\sum_{k(\neq i)}\left(G^{(v_k)}+\frac{1}{2}G^{(v_k)}_{vv}C^{k,k}_{v,v}\right)+K^{(e)}(t), \tag{C6}$$

$$\frac{dm^i_{u_p}}{dt}=F^{(u_{pi})}+\frac{1}{2}F^{(u_{pi})}_{v,v}C^{i,i}_{v,v}+F^{(u_{pi})}_{v,u_p}C^{i,i}_{v,u_p}, \tag{C7}$$

$$\frac{dC^{i,j}_{v,v}}{dt}=2F^{(v_i)}_vC^{i,j}_{v,v}+\sum_{p=2}^{4}F^{(v_i)}_{u_p}(C^{i,j}_{v,u_p}+C^{j,i}_{v,u_p})+[\beta_0^2\delta_{ij}+\beta_1^2(1-\delta_{ij})]+\left(\frac{w}{N-1}\right)\left[\sum_{k(\neq i)}G^{(v_k)}_vC^{j,k}_{v,v}+\sum_{k(\neq j)}G^{(v_k)}_vC^{i,k}_{v,v}\right]+Z^{i,j}_{v,v}, \tag{C8}$$

$$\frac{dC^{i,j}_{v,u_p}}{dt}=(F^{(v_i)}_v+F^{(u_{pi})}_{u_p})C^{i,j}_{v,u_p}+\sum_{q=2}^{4}F^{(v_i)}_{u_q}C^{i,j}_{u_q,u_p}+F^{(u_{pi})}_vC^{i,j}_{v,v}+\left(\frac{w}{N-1}\right)\sum_{k(\neq i)}G^{(v_k)}_vC^{k,j}_{v,u_p}+Z^{i,j}_{v,u_p}, \tag{C9}$$

$$\frac{dC^{i,j}_{u_p,u_q}}{dt}=(F^{(u_{pi})}_{u_p}C^{i,j}_{u_q,u_p}+F^{(u_{qi})}_{u_q}C^{i,j}_{u_p,u_q})+F^{(u_{pi})}_vC^{i,j}_{v,u_q}+F^{(u_{qi})}_vC^{j,i}_{v,u_p}+Z^{i,j}_{u_p,u_q}, \tag{C10}$$

with

$$\begin{aligned}Z^{i,j}_{v,v}=\frac{1}{2}[&F^{(v)}_{vmm}(C^{i,j}_{v,v}C^{j,j}_{m,m}+2C^{i,j}_{v,m}C^{j,j}_{v,m}+C^{i,j}_{v,v}C^{i,i}_{m,m}\\&+2C^{j,i}_{v,m}C^{i,j}_{v,m})+F^{(v)}_{vmh}(C^{i,j}_{v,v}C^{j,j}_{m,h}+C^{i,j}_{v,m}C^{j,j}_{v,h}\\&+C^{i,j}_{v,h}C^{j,j}_{v,m}+C^{i,j}_{v,v}C^{i,i}_{m,h}+C^{j,i}_{v,m}C^{i,i}_{v,h}+C^{j,i}_{v,h}C^{i,i}_{v,m})\\&+F^{(v)}_{vnn}(C^{i,j}_{v,v}C^{j,j}_{n,n}+2C^{i,j}_{v,n}C^{j,j}_{v,n}+C^{i,j}_{v,v}C^{i,i}_{n,n}+2C^{j,i}_{v,n}C^{i,i}_{v,n})\\&+F^{(v)}_{mmm}(C^{i,j}_{v,m}C^{j,j}_{m,m}+C^{j,i}_{v,m}C^{i,i}_{m,m})+F^{(v)}_{nnn}(C^{i,j}_{v,n}C^{j,j}_{n,n}\\&+C^{j,i}_{v,n}C^{i,i}_{n,n})+F^{(v)}_{mmh}(C^{i,j}_{v,h}C^{j,j}_{m,m}+2C^{i,j}_{v,m}C^{j,j}_{m,h}\\&+C^{j,i}_{v,h}C^{i,i}_{m,m}+2C^{j,i}_{v,m}C^{i,i}_{m,h})],\end{aligned} \tag{C11}$$

$$\begin{aligned}Z^{i,j}_{v,u_p}=\frac{1}{2}[&F^{(v)}_{vmm}(C^{i,j}_{v,u_p}C^{i,i}_{m,m}+2C^{i,j}_{m,u_p}C^{i,i}_{v,m})\\&+F^{(v)}_{vmh}(C^{i,j}_{v,u_p}C^{i,i}_{m,h}+C^{i,j}_{m,u_p}C^{i,i}_{v,h}+C^{i,j}_{h,u_p}C^{i,i}_{v,m})\\&+F^{(v)}_{vnn}(C^{i,j}_{v,u_p}C^{i,i}_{n,n}+2C^{i,j}_{n,u_p}C^{i,i}_{v,n})+F^{(v)}_{mmm}C^{i,j}_{m,u_p}C^{i,i}_{m,m}\\&+F^{(v)}_{nnn}C^{i,j}_{n,u_p}C^{i,i}_{n,n}+F^{(v)}_{mmh}(C^{i,j}_{h,u_p}C^{i,i}_{m,m}+2C^{i,j}_{m,u_p}C^{i,i}_{m,h})\\&+F^{(u_p)}_{vvv}C^{i,j}_{v,v}C^{j,j}_{v,v}+F^{(u_p)}_{vvu_p}(C^{i,j}_{v,u_p}C^{j,j}_{v,v}+2C^{i,j}_{v,v}C^{j,j}_{v,u_p})],\end{aligned} \tag{C12}$$

$$\begin{aligned}Z^{i,j}_{u_p,u_q}=\frac{1}{2}[&F^{(u_p)}_{vvv}C^{i,j}_{v,u_q}V^{i,i}_{v,v}+F^{(u_p)}_{vvu_p}(C^{i,j}_{u_p,u_q}C^{i,i}_{v,v}\\&+2C^{i,j}_{v,u_q}C^{i,i}_{v,u_p})+F^{(u_q)}_{vvv}C^{i,j}_{u_p,v}C^{j,j}_{v,v}\\&+F^{(u_q)}_{vvu_q}(C^{i,j}_{u_p,u_q}C^{j,j}_{v,v}+2C^{i,j}_{u_p,v}C^{j,j}_{v,u_q})],\end{aligned} \tag{C13}$$

where $F^{(v_i)}$, $F^{(v_i)}_v=\partial F/\partial v_i$, and $F^{(v_i)}_{v,u_p}=\partial^2F/\partial v_i\partial u_{pi}$ are evaluated for the averages of $(m_v^i,\{m^i_{u_p}\})$, and similar derivatives for $F^{(u_{pi})}$ and $G^{(v_k)}$. Equations given by Eqs. (C6)–(C13) denote the result of the fourth-order moment method. The second-order moment method was applied to a single HH neuron by RT [19,20], whose result is given by Eqs. (C6)–(C10) when we set $i=j=1$, $w=0$, $\beta_1=0$, and $Z_{v,v}=Z_{v,u_p}=Z_{u_p,u_q}=0$. Equations (C6)–(C13) lead to the DMA equation given by Eqs. (45)–(52) and (B1)–(B6) if we adopt the relations as given by Eqs. (A5)–(A7). In particular, in the case of $N=1$, Eqs. (C6)–(C13) are identical with Eqs. (45)–(52) and (B1)–(B6) of the DMA if we read $m^1_\kappa=\mu_\kappa$, $C^{1,1}_{\kappa,\lambda}=\gamma_{\kappa,\lambda}=\rho_{\kappa,\lambda}$, and $Z^{1,1}_{\kappa,\lambda}=X_{\kappa,\lambda}=Y_{\kappa,\lambda}$.

[1] A.L. Hodgkin and A.F. Huxley, J. Physiol. (London) **117**, 500 (1952).
[2] R. FitzHugh, Biophys. J. **1**, 445 (1961).
[3] J. Nagumo, S. Arimoto, and S. Yoshizawa, Proc. IRE **50**, 2061 (1962).
[4] J.L. Hindmarsh and R.M. Rose, Nature (London) **296**, 162 (1982).
[5] Z.F. Mainen and T.J. Sejnowsky, Science **268**, 1503 (1995).
[6] J.P. Segund, J.F. Vibert, K. Pakdaman, M. Stiber, and O. Diez-Martinez, in *Origins; Brain and Self Organization*, edited by K. Pribram (Lawrence Erlbaum Associates, Mahwah, NJ, 1994), pp. 299–331.
[7] J.J. Hopfield, Nature (London) **376**, 33 (1995).
[8] D. Horn and S. Levanda, Neural Comput. **10**, 1705 (1998).
[9] R. van Rullen and S.J. Thorpe, Neural Comput. **13**, 1255 (2001).
[10] C.M. Gray and W. Singer, Proc. Natl. Acad. Sci. U.S.A. **86**, 1698 (1989).
[11] N. Hatsopoulas, C.L. Ojakangas, L. Paninski, and J.P. Donohue, Proc. Natl. Acad. Sci. U.S.A. **95**, 15706 (1998).
[12] R.C. deCharmes and M.M. Merzenich, Nature (London) **381**, 610 (1996).
[13] H. Risken, *The Fokker-Planck Equation: Methods of Solution and Applications*, Springer Series in Synergetics Vol. 18 (Springer-Verlag, Berlin, 1992).
[14] N. Fourcaud and N. Brunel, Neural Comput. **14**, 2057 (2002).
[15] A. Omurtag, B.W. Knight, and L. Sirovich, J. Comput. Neurosci. **8**, 51 (2000).
[16] E. Haskell, D.Q. Nykamp, and D. Tranchina, Nature (London) **12**, 141 (2000).
[17] R. Rodriguez and H.C. Tuckwell, Phys. Rev. E **54**, 5585 (1996).
[18] H.C. Tuckwell and R. Rodriguez, J. Comput. Neurosci. **5**, 91 (1998).
[19] R. Rodriguez and H.C. Tuckwell, BioSystems **48**, 187 (1998).
[20] R. Rodriguez and H.C. Tuckwell, Math. Comput. Modell. **31**, 175 (2000).
[21] H. Hasegawa, Phys. Rev. E **67**, 041903 (2003).
[22] S. Tanabe, S. Sato, and K. Pakdaman, Phys. Rev. E **60**, 7235 (1999).
[23] H. Hasegawa, Phys. Rev. E **61**, 718 (2000).
[24] H. Hasegawa, J. Phys. Soc. Jpn. **69**, 3726 (2000).
[25] Y. Wang and Z.D. Wang, Phys. Rev. E **62**, 1063 (2000).
[26] S. Lee, A. Neiman, and S. Kim, Phys. Rev. E **57**, 3292 (1998).
[27] S. Lee and S. Kim, Phys. Rev. E **60**, 826 (1999).
[28] X. Pei, L. Wilkens, and F. Moss, Phys. Rev. Lett. **77**, 4679 (1996).
[29] T. Kanamaru, T. Horita, and Y. Okabe, J. Phys. Soc. Jpn. **67**, 4058 (1998).
[30] Y. Wang, D.T.W. Chik, and Z.D. Wang, Phys. Rev. E **61**, 740 (2000).
[31] F. Liu, B. Hu, and W. Wang, Phys. Rev. E **63**, 031907 (2000).
[32] H. Hasegawa, Phys. Rev. E **66**, 021902 (2002).
[33] H. Hasegawa, Bull. Tokyo Gakugei Univ., Sect. IV **55**, 5 (2003).
[34] The normalization factor of the coupling term given by Eq. (1) is $(N-1)^{-1}$ in this paper while it is N^{-1} in I; results of the latter are obtainable from those of the former by a replacement of $w \to w(1-1/N)$.
[35] As for the coupling term in Eq. (1), we may adopt an alternative functional form given by $G(v_j)=(v_s-v_j)\alpha(t-t_{oj})$ instead of the sigmoid function, where v_s denotes the synapse reversal potential, t_{oj} the firing time of a neuron j and $\alpha(t)$ is the alpha function [Eq. (57)].
[36] The average (or the expectation value) of an arbitrary function of $Q(\mathbf{z},t)$ is given by $\langle Q(\mathbf{z},t)\rangle = \int \cdots \int d\mathbf{z} Q(\mathbf{z},t)p(\mathbf{z})$, where $p(\mathbf{z})$ denote a probability distribution function for KN-dimensional random variables of $\mathbf{z}=(\{u_{pi}\})$.
[37] S. Tanabe and K. Pakdaman, Biol. Cybern. **85**, 269 (2001).
[38] S. Tanabe and K. Pakdaman, Phys. Rev. E **63**, 031911 (2001).
[39] Fortran programs of DMA for HH neuron ensembles are available at http://www.u-gakugei.ac.jp/~physics/hasegawa.html, or on request to the author.